THE JOURNAL OF PHYSICAL CHEMISTRY A

Article

pubs.acs.org/JPCA

Chlorination of Lanthanum Oxide

Juan P. Gaviría,*[,†,‡] Lucas G. Navarro,[†] and Ana E. Bohé[†,‡,§]

[†]Departamento de Fisicoquímica y Control de Calidad, Complejo Tecnológico Pilcaniyeu, Centro Atómico Bariloche, Comisión Nacional de Energía Atómica, Av. Bustillo km 9500 (8400), S.C. de Bariloche, Río Negro, Argentina

[‡]Consejo Nacional de Investigaciones Científicas y Técnicas, Argentina

[§]Centro Regional Universitario Bariloche, Universidad Nacional del Comahue, Argentina

ABSTRACT: The reactive system $La_2O_3(s)-Cl_2(g)$ was studied in the temperature range 260−950 °C. The reaction course was followed by thermogravimetry, and the solids involved were characterized by X-ray diffraction, scanning electron microscopy, and energy dispersive spectroscopy. The results showed that the reaction leads to the formation of solid LaOCl, and for temperatures above 850 °C, the lanthanum oxychloride is chlorinated, producing $LaCl_3(l)$. The formation of the oxychloride progresses through a nucleation and growth mechanism, and the kinetic analysis showed that at temperatures below 325 °C the system is under chemical control. The influence of diffusive processes on the kinetics of production of LaOCl was evaluated by studying the effect of the reactive gas flow rate, the mass of the sample, and the chlorine diffusion through the boundary layer surrounding the solid sample. The conversion curves were analyzed and fitted according to the Johnson−Mehl−Avrami description, and the reaction order with respect to the chlorine partial pressure was obtained by varying this partial pressure between 10 and 70 kPa. The rate equation was obtained, which includes the influence of the temperature, chlorine partial pressure, and reaction degree.

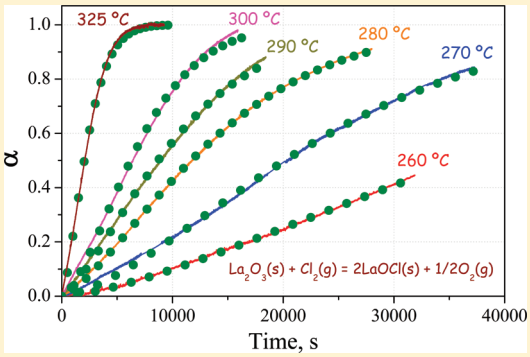

1. INTRODUCTION

Direct chlorination is a potential dry method for the production of rare earth chlorides, which allows further isolation of metals from ores and concentrates.[1] The combination of chlorination and chemical vapor transportation is a method for recovery and separation of rare earths from oxide mixtures and sludges.[2,3]

Although there are several studies about chlorination with NH_4Cl[4,5] and CCl_4[6−10] of lanthanum oxide and other lanthanum compounds, none have paid special attention to the kinetics, mechanism, and structural changes and there are no published reports about *direct chlorination of lanthanum oxide with gaseous chlorine*.

The aim of this work is to continue with the kinetic research on direct chlorination of rare earth oxides,[11−14] and to study the chlorination of La_2O_3 in order to determine the rate equation, the mechanism of the reaction, and the kinetics parameters.

An electro-balance was used to follow the course of the reaction, and the resulting solids were analyzed with X-ray diffraction (XRD), scanning electron microscopy (SEM), and energy dispersive spectroscopy (EDS).

The studies showed that LaOCl is the only existing solid phase after direct chlorination of La_2O_3 at the working temperature range. This compound has several potential uses as it is becoming of great interest within various industries due to its capability and potential to be used as a catalyst in the oxidative methane coupling, oxidative dehydrogenation of ethane, oxidative chlorination of methane, conversion of ethane and ethylene to vinyl chlorides and in the destruction of chlorinated hydrocarbons, toxins of the environment.[8,15−19] Its nanomaterial can be used as a luminescent material and gas sensor.[20−22]

2. MATERIALS AND METHODS

The materials used were a lanthanum hydroxide [$La(OH)_3$] powder 99.98% (Fluka), chlorine (Cl_2) 99.8% purity (Indupa, Bahía Blanca, Argentina), and argon 99.99% purity (AGA, Buenos Aires, Argentina). The particle size distribution of the $La(OH)_3$ powder measured by laser diffraction showed that 90% v/v of the particles have a size lower than 10 μm and 45% v/v have sizes between 2 and 6 μm (Mastersizer, Malvern Instruments Limited).

Solids were analyzed by X-ray diffraction (Philips PW 1310-01, with Ni filtered Cu Kα radiation), scanning electron microscopy (SEM 515, Philips Electronic Instruments), and energy dispersive spectroscopy (EDAX Genesis 2000).

The chlorination reactions were carried out using a *thermogravimetric system*.[23] It consists of an electro-balance (Cahn 2000, Cahn Instruments, Inc., Cerritos, CA) adapted to work with corrosive atmospheres, a vertical tube furnace, a gas line, and a data acquisition system. The sensitivity of the system is ±0.01 mg while operating at 1000 °C under a gas flow rate of 9 L/h (measured at normal temperature and pressure). Each

Received: July 26, 2011
Revised: January 25, 2012
Published: January 25, 2012

   dx.doi.org/10.1021/jp210457r | *J. Phys. Chem. A* 2012, 116, 2062−2070

sample was placed in a cylindrical silica glass crucible (7.8 mm inner diameter and 3.3 mm deep), which hangs from one of the arms of the electro-balance through a silica glass wire. The reactor is a hang-down silica glass tube (4.6 cm inner diameter) which carries the gases (Ar/Cl_2) to the sample. The temperature was measured using a Pt−Pt (10% Rh) encapsulated thermocouple which was placed 5 mm below the crucible. Flows of Ar and Cl_2 were controlled by flow meters, and they were dried by passing them through silica gel and $CaCl_2$, respectively. The La_2O_3 samples (product of the $La(OH)_3$ decomposition) were heated in flowing Ar until the reaction temperature was reached. After temperature stabilization, chlorine was admitted into the reactor while mass changes were monitored every 2.5 s. The acquired data were carefully analyzed to determine the reaction zero time.

2.1. Production of La_2O_3 by $La(OH)_3$ Decomposition. The *lanthanum oxide* used in the chlorinations was obtained by $La(OH)_3$ thermal decomposition under Ar atmosphere. The thermal treatment was a heating of 40 min until 850 °C and 20 min at this temperature. Figure 1 shows a thermogravimetric

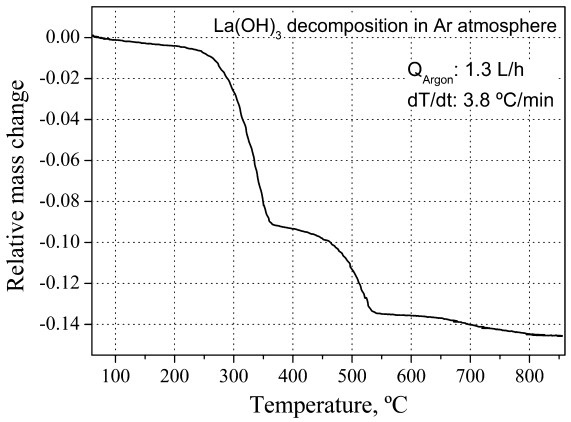

Figure 1. Thermo-gravimetric curve of $La(OH)_3$ decomposition.

curve of the $La(OH)_3$ decomposition. The curve indicates three steps of weight loss, with these steps being associated with the following reactions:

$$La(OH)_3(s) \rightarrow LaOOH(s) + H_2O(g) \quad [\approx 240-360°C] \tag{1}$$

$$LaOOH(s) \rightarrow {}^1/_2La_2O_3(s) + {}^1/_2H_2O(g) \quad [\approx >440°C] \tag{2}$$

$$La_2O_2CO_3(s) \rightarrow La_2O_3(s) + CO_2(g) \quad [\approx >630°C] \tag{3}$$

The presence of a small amount of lanthanum oxide carbonate ($La_2O_2CO_3$) in the starting material and the formation of LaOOH during the decomposition was verified by XRD ($La_2O_2CO_3$: reference pattern, 37-804;[24] crystal system, hexagonal; space group, $P6_3/mmc$; space group number, 194. LaOOH: reference pattern, 19-656;[24] crystal system, monoclinic; space group, $P2_1/m$; space group number, 11).

The final relative mass loss of the curve corresponds to the global reaction of La_2O_3 production by $La(OH)_3$ decomposition (≈0.142). The final product of the treatment was analyzed by XRD obtaining only the diffraction lines of La_2O_3 (reference pattern, 73-2141;[24] crystal system, hexagonal; space group, $P\text{-}3m1$; space group number, 164). These results are in good agreement with those obtained by Neumann et al.[25]

The sample of La_2O_3 obtained was left in the reactor and subsequently chlorinated.

3. RESULTS AND DISCUSSION

3.1. Thermodynamic Considerations. The following reactions are possible in the $La_2O_3-Cl_2$ reactive system:

$$La_2O_3(s) + Cl_2(g) \rightarrow 2LaOCl(s) + {}^1/_2O_2(g) \tag{4}$$

$${}^1/_3La_2O_3(s) + Cl_2(g) \rightarrow {}^2/_3LaCl_3(s, l) + {}^1/_2O_2(g) \tag{5}$$

$$LaOCl(s) + Cl_2(g) \rightarrow LaCl_3(s, l) + {}^1/_2O_2(g) \tag{6}$$

$$LaOCl(s) \rightarrow {}^1/_3La_2O_3(s) + {}^1/_3LaCl_3(s, l) \tag{7}$$

The physical properties reported for lanthanum compounds are the following: La_2O_3 (T_m = 2313 °C);[26] LaOCl (T_d = 934 °C (in vacuum));[27] $LaCl_3$ (T_m = 858 °C, T_v = 1747 °C).[26] T_m, T_d, and T_v are the melting, decomposition, and vaporization temperatures.

Figure 2 shows the temperature dependence of the standard Gibbs free energy for reactions 4−7 between 0 and 1000 °C.

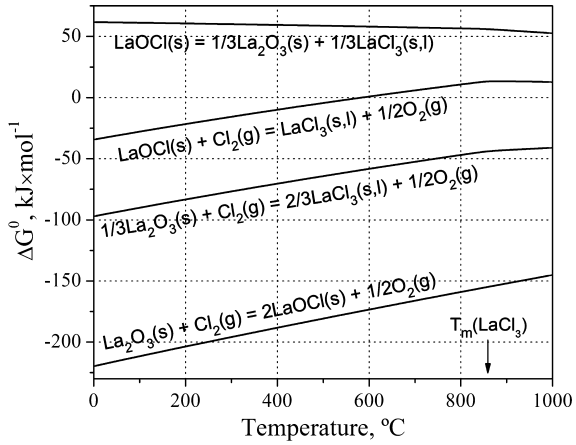

Figure 2. Standard Gibbs free energy (per mole of chlorine) vs temperature for reactions involved in the $La_2O_3-Cl_2(g)$ system. T_m is the melting point of $LaCl_3$ (858 °C).

The calculations were performed with HSC 6.12 Software,[28] and the reactions were taken per mole of chlorine.

The results can be compared, assuming that the reactions are independent from each other. The curves show that the chlorination reactions of La_2O_3 to produce LaOCl and $LaCl_3$ have negative ΔG^0 values, and the formation of the oxychloride is thermodynamically more feasible to occur. Then, LaOCl could be chlorinated (reaction 6) or decomposed (reaction 7). The chlorination of LaOCl has negative ΔG^0 values for temperatures below 580 °C, and has lower ΔG^0 values than the LaOCl decomposition reaction (compared per mole of LaOCl).

The phase stability diagram of the La−O−Cl system at 400 °C is shown in Figure 3.[28] The axes are the partial pressure of O_2 and Cl_2. The diagram indicates that La_2O_3 and $LaCl_3$ do not have a thermodynamic equilibrium, and LaOCl has to be formed previous to the formation of $LaCl_3$ from La_2O_3.

3.2. Nonisothermal Chlorination Experiments. Nonisothermal chlorination experiments were carried out in order

dx.doi.org/10.1021/jp210457r | J. Phys. Chem. A 2012, 116, 2062−2070

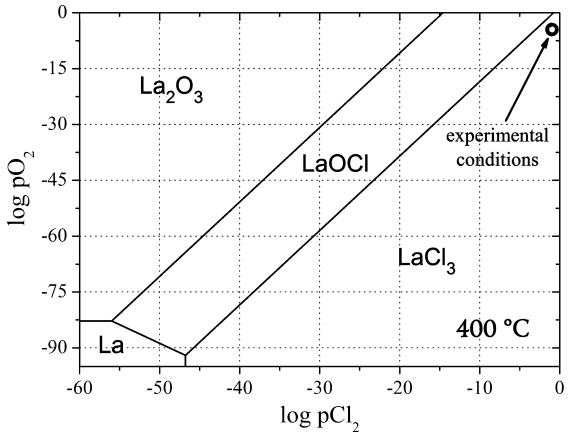

Figure 3. Phase stability diagram of the La−O−Cl system at 400 °C. Experimental conditions: pCl_2, 35 kPa (0.35 bar); pO_2, 10^{-6} bar (1 ppm).

to determine both the reactivity with temperature and the reaction products. Figure 4 shows the *relative mass change* ($\Delta m/m_0$) vs *temperature* for this system under Ar−Cl_2 atmosphere from 100 to 1000 °C.

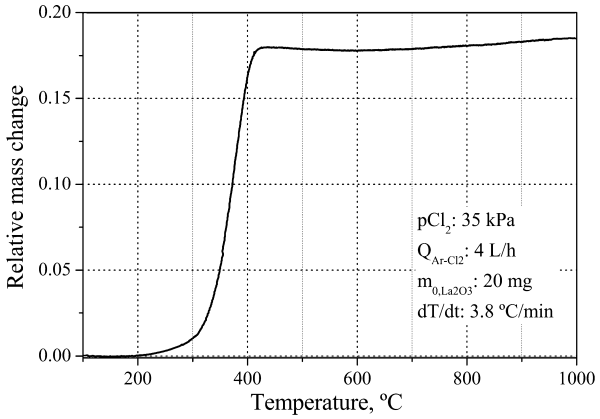

Figure 4. Nonisothermal thermo-gravimetry of La_2O_3 chlorination.

The sample undergoes a mass gain starting from a temperature of about 260 °C. The mass change rate increases quickly until the mass change reaches a maximum value of $\Delta m/m_0 = 0.18$, very close to the relative mass change expected for reaction 4. Figure 5 shows the XRD patterns for the unreacted La_2O_3 (obtained by $La(OH)_3$ decomposition), the residue after nonisothermal chlorination, and the LaOCl pattern (reference pattern, 8-477;[24] crystal system, tetragonal; space group, *P4/nmm*; space group number, 129). The solid residue only showed the LaOCl diffraction lines, and the analyses performed by EDS were consistent with the chemical formula of this compound. The EDS analyses were performed over three samples chlorinated at 350, 850, and 950 °C. The average composition, taking into account only La and Cl, for six measurements (two for each sample) was 52 ± 3 for La and 48 ± 3 for Cl (% at). Lanthanum oxychloride is a not hygroscopic white powder and is stable when exposed to air.[29]

The thermodynamical analysis showed that LaOCl is the compound thermodynamically more feasible to be formed from La_2O_3 chlorination (Figure 2) and $LaCl_3$ is the more stable final product under the experimental conditions used (Figure 3). The DRX analyses of the final condensed products in the whole

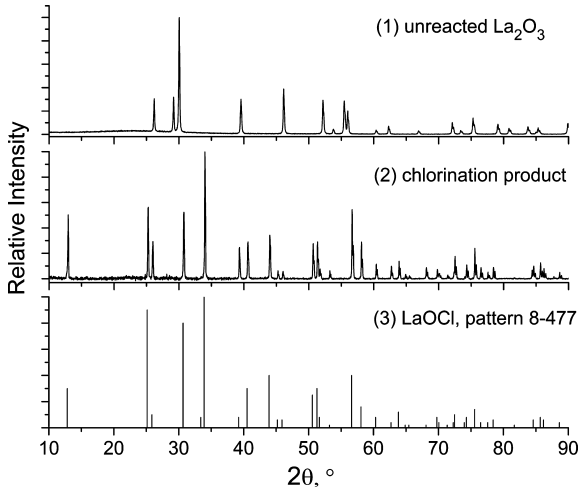

Figure 5. Diffraction patterns for (1) unreacted La_2O_3; (2) product of the nonisothermal chlorination; (3) LaOCl reference pattern.[24]

temperature range (260−950 °C) showed that LaOCl was the only phase present. This behavior is indicating that conversion of LaOCl to $LaCl_3$ is kinetically limited.

Therefore, the results indicate that the reaction taking place is reaction 4:

$$La_2O_3(s) + Cl_2(g) \rightarrow 2LaOCl(s) + {}^1/_2O_2(g) \quad (4)$$

The conversion degree is defined as

$$\alpha = \alpha_{La_2O_3} = \frac{m_0 - m_{tLa_2O_3}}{m_0} \quad (I)$$

where m_0 and $m_{tLa_2O_3}$ are the weights of La_2O_3 at *zero* time and time *t*, respectively.

The *mass change measured in the thermo-balance* (Δm) includes the weights of La_2O_3 and LaOCl. After relating these weights with conversion, an expression is obtained for α as a function of Δm:

$$\alpha = \frac{\left(\frac{\Delta m}{m_0}\right)}{\left(2\frac{PM_{LaOCl}}{PM_{La_2O_3}} - 1\right)} \cong \left(\frac{\Delta m}{m_0}\right)\frac{1}{0.169} \quad (II)$$

where 0.169 is the final relative mass change of reaction 4.

The formation of LaOCl as the intermediate solid reaction product in the production of $LaCl_3$ by La_2O_3 chlorination with NH_4Cl and CCl_4 has been observed by several authors (NH_4Cl;[4,5] CCl_4[6−9]).

3.3. Isothermal Thermo-Gravimetric Experiments. The isothermal chlorination experiments performed at temperatures between 260 and 950 °C (m_{0,La_2O_3}, 10 mg; pCl_2, 35 kPa; Q_{Ar-Cl_2}, 4 L/h) showed that the system has different kinetic behavior depending on the temperature range (Figure 6). For temperatures below 325 °C, the conversion curves have a sigmoidal shape, which is typical for *nucleation and growth* transformations (Figure 14). This type of process has been observed for the formation of REOCl by RE_2O_3 chlorination (RE: rare eath) (samarium,[13] yttrium[14,30,31]). For temperatures above 350 °C, the initial reaction rate is the fastest of the overall reaction, which is a different behavior compared to the reactions performed at lower temperatures where the reaction rate at the

dx.doi.org/10.1021/jp210457r | J. Phys. Chem. A 2012, 116, 2062−2070

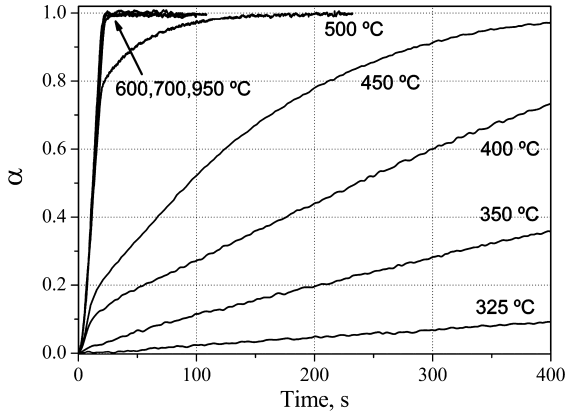

Figure 6. Isothermal chlorination of La_2O_3.

beginning of the reaction is nearly zero (transformations which follow a nucleation and growth mechanism have a theoretical initial rate equal to zero).

For temperatures in the range 350−500 °C, the beginning of the reaction proceeds through a *fast stage* and the formation of LaOCl is subsequently completed by a slower kinetic stage. For temperatures above 600 °C, the production of LaOCl is fully performed by the *fast stage*, being rate independent of the temperature.

Chlorination experiments performed at temperatures above 850 °C showed that after the formation of LaOCl the system progresses with mass loss (Figure 7). The XRD analyses of the solid residues of these reactions showed that LaOCl is the only compound present.

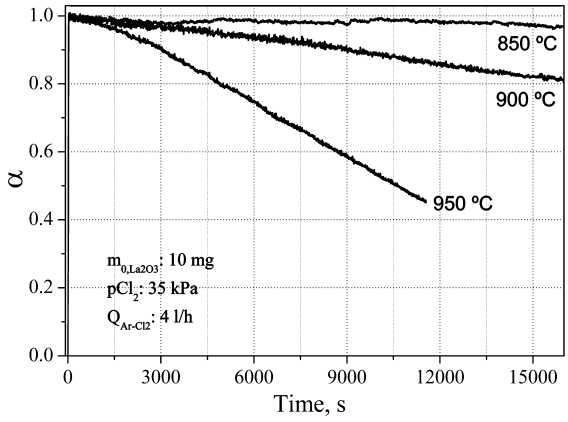

Figure 7. Isothermal chlorinations of La_2O_3 above 850 °C.

Samples of LaOCl treated at 950 °C in argon atmosphere for 4 h showed no mass changes. After this treatment, the samples were analyzed by XRD, obtaining only the LaOCl diffraction lines.

These results are indicating that weight loss is caused by a reaction between LaOCl and Cl_2, as can be reaction 6. The lanthanum trichloride formed is in liquid state, with the vapor pressures being 4.7×10^{-5} and 3.7×10^{-4} bar at 850 and 950 °C, respectively.[28] The reaction is carried out under a continuous flow which removes the vapor in equilibrium with the liquid.

Then, reactions involved in the La_2O_3−Cl_2 system are the following:

$$La_2O_3(s) + Cl_2(g) \rightarrow 2LaOCl(s) + {}^1/_2O_2(g) \quad (4)$$

$$LaOCl(s) + Cl_2(g) \rightarrow LaCl_3(l) + {}^1/_2O_2(g) \quad (6)$$

$$LaCl_3(l) = LaCl_3(g) \quad (8)$$

Reactions 6 and 8 occur at temperatures above 850 °C. Reaction 8 is faster than reaction 6, causing $LaCl_3$ to not be present as a condensed product after the chlorinations.

3.4. Morphological Analysis. Figure 8 shows SEM images with 10000× magnification of (a) starting $La(OH)_3$, (b) La_2O_3 obtained by $La(OH)_3$ decomposition, (c) LaOCl produced at 325 °C, and (d) LaOCl produced at 950 °C. It can be observed that there are few morphological differences between $La(OH)_3$ and La_2O_3. The sample of LaOCl formed at 325 °C has a smaller grain size than the La_2O_3, which is in accordance with the behavior expected for a nucleation and growth mechanism (several LaOCl nuclei are formed inside the La_2O_3 grains). The morphology of the lanthanum oxychloride is quite different at temperatures below and above the melting point of $LaCl_3$ (858 °C). At temperatures below 858 °C, the LaOCl grains are smaller than those obtained at higher temperatures (Figure 8c and d).

3.5. Effect of the Gas Phase Mass Transfer. The kinetics in gas−solid reactions can be affected by two *gas phase* phenomena: *convective mass transfer through the boundary layer* and *reacting gas supply*.[32] The first process is analyzed by comparing the *calculated* chlorine molar flow diffusing through the boundary layer surrounding the solid sample with the *measured* chlorine molar flow (obtained from thermo-gravimetric curves and assuming a given reaction stoichiometry). The second one can be evaluated by studying the influence of the total flow rate (supply rate of chlorine) on the reaction rate.

The molar flow of Cl_2 by diffusion (and assuming no starvation) can be estimated by using the Ranz−Marshall correlation[33,34] (the development of eq III is detailed in ref 31):

$$\frac{dn_{Cl_2}}{dt} = \frac{D_{Ar-Cl_2}(2 + 0.6N_{Re}{}^{1/2}N_{Sc}{}^{1/3})}{L} \frac{(P_{Cl_2,0} - P_{Cl_2,S})}{R_gT}A \quad (III)$$

where dn_{Cl_2}/dt is the chlorine molar flow, D_{Ar-Cl_2} is the binary diffusion coefficient for Ar−Cl_2, $N_{Re} = U{\cdot}L/\nu$ represents the Reynolds number (U is the linear fluid velocity, and ν is the kinematic viscosity), $N_{Sc} = \nu/D_{Ar-Cl_2}$ is the Schmidt number, L is the sample characteristic dimension (taken as the crucible diameter), A is the sample external surface (considered equal to the crucible transversal area), R_g is the gas constant, P_{Cl_2} is the chlorine partial pressure, and the subscripts 0 and S represent the bulk gas stream and sample surface, respectively.

The values of dn_{Cl_2}/dt calculated by eq III and those obtained from thermo-gravimetric curves, for temperatures between 300 and 700 °C, are shown in Table 1. Reaction 4 was assumed as irreversible, since the values of the equilibrium constants are 7.07×10^{17} and 5.48×10^{7} at 300 and 800 °C, respectively.[28] Therefore, the value of $P_{Cl_2,S}$ employed in the calculation is zero. The ν and D_{Ar-Cl_2} values were obtained from the Chapman−Enskog theory.[35,36] The experimental conditions considered were $pCl_2 = P_{Cl_2,0}$, 35 kPa; Q_{Ar-Cl_2}, 4 L/h.

Equation III gives approximate values of dn_{Cl_2}/dt. This equation is valid for a pellet in a freely flowing gas and not for a sample contained in a crucible. Hills[32] and Hakvoort[37] con-

dx.doi.org/10.1021/jp210457r | J. Phys. Chem. A 2012, 116, 2062−2070

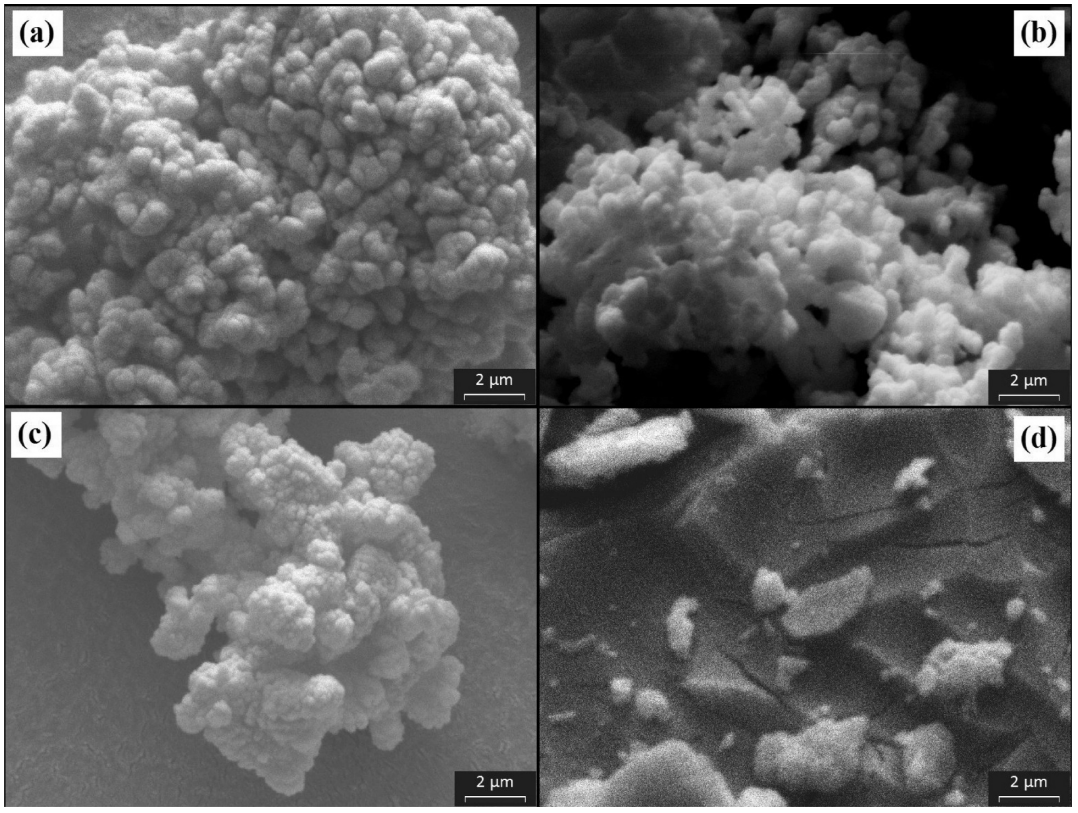

Figure 8. SEM images of (a) starting $La(OH)_3$; (b) La_2O_3 produced by $La(OH)_3$ decomposition; (c) LaOCl formed at 325 °C; (d) LaOCl formed at 950 °C.

Table 1. Comparison between Calculated and Measured Molar Flow of Chlorine[a]

T (°C)	(1) dn_{Cl_2}/dt [calculated][b] (mol of Cl_2/s)	(2) dn_{Cl_2}/dt [measured][c] (mol of Cl_2/s)	(1)/(2)
300	4.05×10^{-6}	2.72×10^{-9}	1487
350	4.31×10^{-6}	3.30×10^{-8}	131
400	4.55×10^{-6}	2.40×10^{-7}	19
500	5.02×10^{-6}	1.22×10^{-6}	4.1
700	5.88×10^{-6}	1.68×10^{-6}	3.5

[a]Data used for the calculations: L = 0.74 cm; A = 0.43 cm^2; pCl_2 = 35 kPa; Q_{Ar-Cl2} = 4 L/h. [b]Calculated from eq III. [c]Obtained from the thermogravimetric curves at the higher slope (stoichiometry of reaction 4).

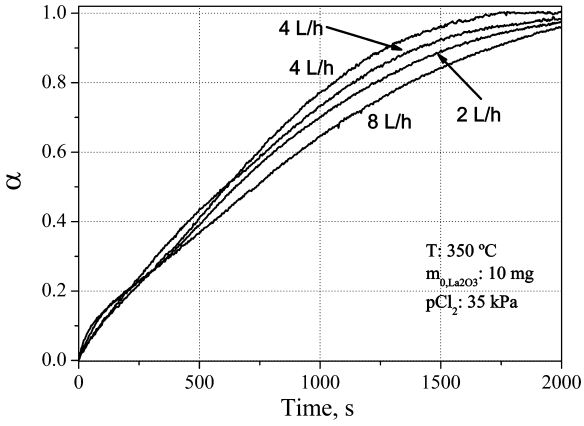

Figure 9. Effect of $Ar-Cl_2$ flow rate on the kinetics of La_2O_3 chlorination at 350 °C. Two curves of 4 L/h are presented to show the reproducibility of the system.

cluded that values obtained using the Ranz and Marshall correlation are more than 1 order of magnitude higher than mass transfer rates for samples contained within crucibles. The criterion used in this work to conclude that the convective mass transfer of chlorine to the surface of the sample is not influencing the reaction rate is when the measured chlorine flow is at least 2 orders of magnitude smaller than the one obtained by using eq III. The results shown in Table 1 indicate that for temperatures below 350 °C the reaction kinetics are not affected by this diffusive process.

Figure 9 shows the influence of the total flow rate on the rate of La_2O_3 chlorination at 350 °C, using Q_{Ar-Cl_2} between 2 and 8 L/h. The difference between the conversion curves is similar to the experimental scattering, and it can be concluded that the supply rate of chlorine is not influencing the kinetics at this temperature. Two curves of 4 L/h are presented to show the reproducibility of the system.

3.6. Mass Transfer through the Interparticle Voids. Diffusion of the gas species (reactants and products) through pores between solid particles can affect the reaction rate. This process was analyzed by studying the effect of the reaction bed thickness, which was varied by changing the mass of La_2O_3. The reaction rate decreases as the bed thickness increases when the interparticle void diffusion is playing a role in the rate control.

Figure 10 shows thermo-gravimetric curves of chlorination experiments performed at 325 °C and initial masses of 2 and 10 mg. The reaction rate does not depend on the sample size at this temperature; therefore, the mass transfer through the

dx.doi.org/10.1021/jp210457r | J. Phys. Chem. A 2012, 116, 2062–2070

interparticle voids is not affecting the overall reaction rate and hence an initial mass of 10 mg was used in the kinetic analysis.

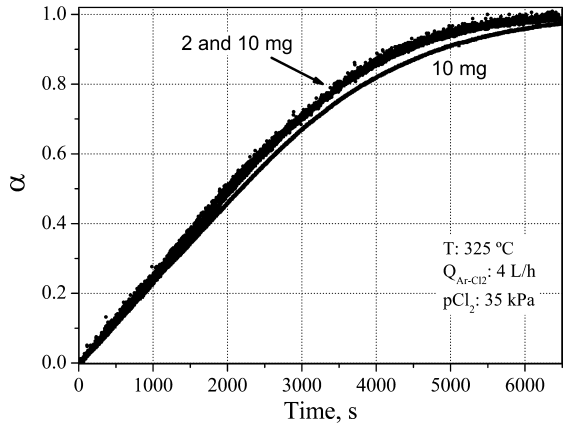

Figure 10. Effect of the initial mass of La_2O_3 on reaction rate at 325 °C.

3.7. Kinetic Analysis for $T \geq 350$ °C. For temperatures above 350 °C, the beginning of the reaction proceeds by a *fast stage*. The kinetics of this stage are affected by the gas phase mass transfer (Table 1, section 3.5); therefore, it is not possible to obtain intrinsic kinetic parameters.

The extension of the fast stage is raised as the temperature (Figure 6) and initial mass are increased. Figure 11 shows the effect of the initial mass of La_2O_3 on the kinetics of chlorination at 450 °C. The extension of the fast stage is α = 0.19, 0.74, and 0.97 for m_0 = 10, 30, and 40 mg, respectively. The same behavior was observed at 500 °C. Figure 11 also shows that the

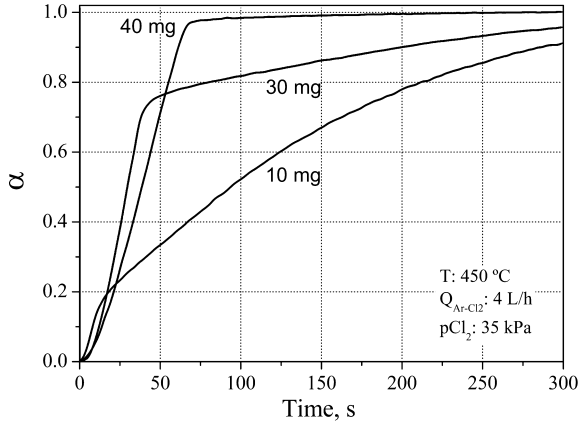

Figure 11. Effect of the mass sample on the kinetics of La_2O_3 chlorination at 450 °C.

time necessary to reach a given conversion depends on the initial mass. For example, a value of α = 0.91 is reached in 300 and 62 s for 10 and 40 mg, respectively.

This behavior is not the most common in gas−solid kinetics. An increment in the reaction bed thickness generally causes the following, depending on the relative importance of the diffusion through the sample pores: (1) a diminution in the reaction rate for systems affected by this diffusion; (2) no change in the kinetics for systems which are not influenced by this process transfer. The increase of the fast stage extension and the reaction rate with the initial mass could be related to the formation of *highly reactive gas intermediates*. The chlorine radical (Cl•) is a probable species to be produced in the La_2O_3−Cl_2 interaction. The chlorine radicals react readily with the oxide to form the oxychloride. As the reaction thickness of the bed increases, the reaction probability before the recombination to form Cl_2 increases. When the reaction thickness diminishes, the radicals have a lower residence time in the bed and the probability of escaping from the sample is higher. Although the behavior can be explained with the proposal of the chlorine radical formation, the presence of this species should be demonstrated. Pasquevich et al.[38,39] observed the same kinetic behavior in the carbochlorination of ZrO_2 (enhancement of the conversion with the increase of the initial mass) and verified by modulated-beam mass spectroscopy the formation of chlorine radicals.

3.8. Kinetic Analysis and Determination of the Equation Rate for $T \leq 325$ °C. The intrinsic kinetic parameters of La_2O_3 chlorination that produces LaOCl and O_2 (reaction 4) are determined in this section. The results analyzed in previous sections showed that the reaction at temperatures below 325 °C follows a unique kinetic behavior and the reaction rate is not affected by gas phase and interparticle void mass transfers (Q_{Ar-Cl_2}, 4 L/h; m_0, 10 mg). Therefore, the kinetics are under chemical control and the reaction rate can be expressed as a *function of separate variables* (T, p, α):

$$\frac{d\alpha}{dt} = k(T)F(pCl_2)G(\alpha) \qquad \text{(IV)}$$

where $k(T)$ refers to an Arrhenius equation, $F(pCl_2)$ expresses the dependence of reaction rate on pCl_2 (it is related to the adsorption/desorption phenomena), and $G(\alpha)$ is a function that describes the morphological evolution of the solid reactant.

3.8.1. Reaction Order with Respect to pCl_2. Figure 12 shows the effect of the chlorine partial pressure on the reaction rate at 300 °C, varying pCl_2 between 10 and 70 kPa.

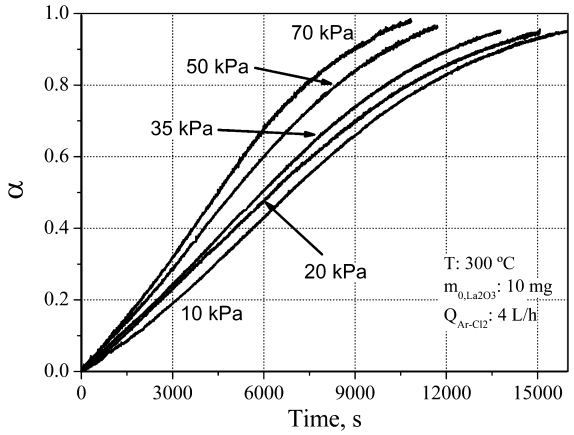

Figure 12. Effect of chlorine partial pressure on the reaction rate of La_2O_3 chlorination at 300 °C.

The reaction order is obtained from the integration of eq IV between $\alpha = 0$ and $\alpha = \alpha$ and $t = 0$ and $t = t$. The temperature is constant (300 °C), and it is assumed that dependence on α and pCl_2 can be separated.

$$\int \frac{d\alpha}{G(\alpha)} = \int k(T)F(pCl_2)\,dt \qquad \text{(V)}$$

$$g(\alpha = \alpha) - g(\alpha = 0) = k(T)F(pCl_2)t(\alpha) \qquad \text{(VI)}$$

dx.doi.org/10.1021/jp210457r | J. Phys. Chem. A 2012, 116, 2062−2070

where $g(\alpha)$ is commonly called the *integrated conversion function* and $t(\alpha)$ is the time to reach a conversion degree α at a given temperature and reactive gas partial pressure.

Assuming that $F(pCl_2) = B{\cdot}pCl_2{}^x$:

$$g(\alpha) - g(0) = k(T)Bp\mathrm{Cl}_2{}^x t(\alpha) \quad \text{(VII)}$$

$$1/t(\alpha) = \frac{k(T)B}{g(\alpha) - g(0)} p\mathrm{Cl}_2{}^x \quad \text{(VIII)}$$

$$-\ln t(\alpha) = \ln\left[\frac{k(T)B}{g(\alpha) - g(0)}\right] + x \ln p\mathrm{Cl}_2 \quad \text{(IX)}$$

The function inside brackets, at constant temperature, depends only on α:

$$-\ln t(\alpha) = H(\alpha) + x \ln p\mathrm{Cl}_2 \quad \text{(X)}$$

The reaction order for a given α and T is obtained by plotting $-\ln t(\alpha)$ vs pCl_2 and calculating the slope of the curve. Figure 13 shows these plots, obtaining an average value of 0.23. It was considered an experimental scattering error of 10% in the time to reach a given conversion.

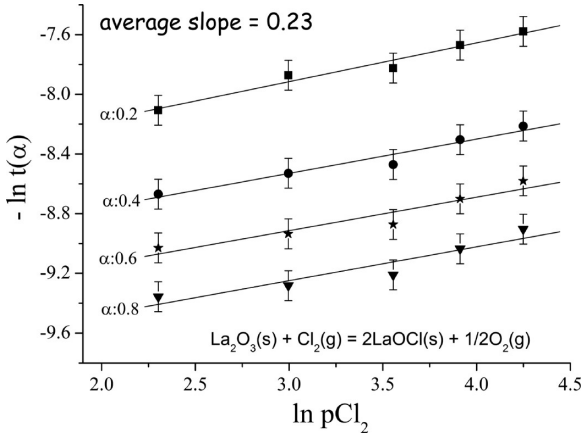

Figure 13. Plot of eq X at different conversions of curves shown in Figure 12.

3.8.2. Reaction Model. The conversion curves were fitted according to the *Johnson–Mehl–Avrami (JMA) model*, which has been developed for isothermal transformations.[40−43] This model proposes that the reaction degree has the following dependence on the reaction time:

$$\alpha = 1 - \exp[-K(T)t]^n \quad \text{(XI)}$$

$$K = K_0 \exp\left(-\frac{E_a}{R_g T}\right) \quad \text{(XII)}$$

where $K(T)$ is the global rate constant (different from $k(T)$ in eq IV, which is the intrinsic rate constant), K_0 is the pre-exponential factor, E_a is the effective activation energy, and n is the JMA exponent. The parameters K_0, E_a, and n depend on the *nucleation and growth mechanisms*.

The conversion curves at $T \leq 325$ °C were fitted with eq XI, and Table 2 shows the values of n, K, and r^2 obtained from a nonlinear least-squares fitting. Figure 14 shows the experimental curves (*line graphs*) and the fitted curves (*scatter graphs*), showing the good fit between them.

Table 2. Values of n and K Obtained from a Nonlinear Least Squares Fitting of Conversion Curves with eq XI

T (°C)	n	K (s^{-1})	r^2
260	1.471 ± 0.001	(2.148 ± 0.001) × 10^{-5}	0.9988
270	1.525 ± 0.001	(3.901 ± 0.002) × 10^{-5}	0.9981
280	1.396 ± 0.0005	(6.577 ± 0.001) × 10^{-5}	0.9998
290	1.377 ± 0.001	(8.804 ± 0.003) × 10^{-5}	0.9976
300	1.540 ± 0.002	(1.266 ± 0.007) × 10^{-4}	0.9958
325	1.457 ± 0.002	(3.817 ± 0.003) × 10^{-4}	0.9981

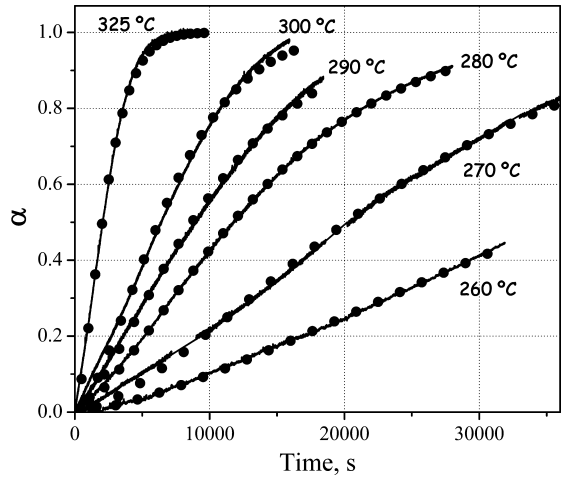

Figure 14. Fits of the conversion curves with the JMA equation. Line graphs, experimental curves; scatter graphs, calculated curves.

The average value of n obtained was 1.461 ± 0.066. The value of n is dependent on the nucleation and growth mechanisms. The types of growth considered in the JMA description are *volume diffusion* controlled and *interface* controlled. *Interface* controlled can occur in the absence of compositional changes (e.g., in cases of allotropic phase transformations), and *volume diffusion* can occur upon phase transformations where long-range compositional changes take place.[44] The transformation analyzed in this work is the nucleation and growth of LaOCl from the chlorination of La_2O_3. This process involves compositional changes; therefore, we can assume the *LaOCl nuclei are growing controlled by volume diffusion*.

The nucleation models taken into account in the JMA description are *continuous nucleation* and *site saturation*. Kempen et al.[44] demonstrated numerically that intermediate values of the JMA exponents are possible for combination of the different nucleation models and volume diffusion growth: (I) between 1/2 (one-dimensional growth) and 3/2 (three-dimensional growth) for site saturation and (II) between 3/2 (one-dimensional growth) and 5/2 (three-dimensional growth) for continuous nucleation.

The obtained value for the JMA exponent could be consistent with a three-dimensional growth and site saturation. Figure 15 shows a magnification of Figure 8c, showing the detail of the LaOCl nuclei. It can be observed that these nuclei had a three-dimensional growth. The nucleation mechanism of site saturation assumes that the number of supercritical nuclei does not change during transformation; all nuclei are present at zero time. A possible mechanism, coherent with the results analyzed in section 3.7, is the following: at the beginning of the reaction, the Cl_2 molecule is destructively adsorbed and some

dx.doi.org/10.1021/jp210457r | J. Phys. Chem. A 2012, 116, 2062−2070

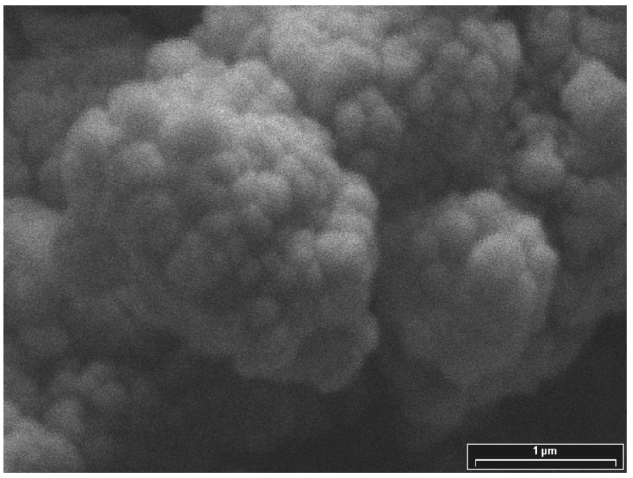

Figure 15. SEM image of LaOCl obtained from La_2O_3 chlorination at 325 °C.

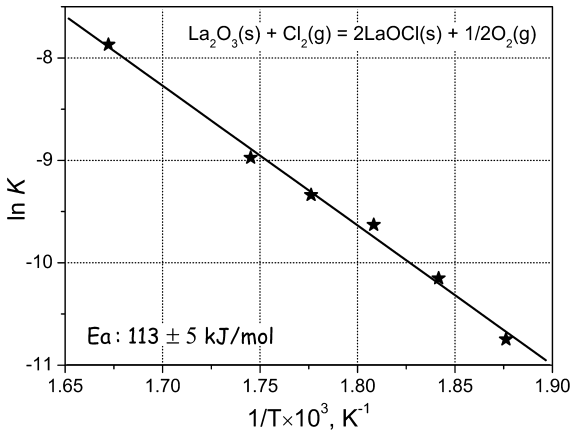

Figure 16. Plot of ln K vs $1/T$. The K values were obtained from the JMA analysis.

Table 3. Activation Energies for Reaction $RE_2O_3(s) + Cl_2(g) = 2REOCl(s) + {}^1/_2O_2(g)$ (RE: Rare Earth)

RE	E_a (kJ/mol)	temperature range (°C)	reference
La	113 ± 5	260–325	this work
Sm	130 ± 5	270–350	12, 13
Y	187 ± 3	575–800	14

of the generated Cl atoms diffuse into the La_2O_3 bulk. These atoms react and produce all LaOCl nuclei, which subsequently grow.

Lanthanum oxide is widely used as a *reactive substrate* in the low temperature destruction of chlorinated hydrocarbons.[6−10,16,17] A feature of these reactions is the facile oxygen diffusion from the bulk to the surface to undergo O/Cl exchange.[8]

The function $G(\alpha)$ can be obtained by combining eqs IV and XI, and the average value of n in the range of temperature analyzed was 1.46:

$$G(\alpha) = n(1-\alpha)[-\ln(1-\alpha)]^{(n-1)/n} \qquad (n = 1.46) \tag{XIII}$$

3.8.3. Activation Energy. The activation energy in the temperature range of 260−325 °C was calculated from the values of the global rate constant $K(T)$ obtained by the application of the JMA model (Table 2). Figure 16 shows the plot of ln K vs $1/T$, from which a value for the *intrinsic activation energy* of 113 ± 5 kJ/mol was obtained. Table 3 shows the comparison with the intrinsic activation energies obtained for the same reaction using other rare earths. These reactions were studied in the *same experimental system*. The lower E_a belongs to the *lanthanum oxide* chlorination, being consistent with the use of this compound for the destruction of chlorinated hydrocarbons.

4. CONCLUSIONS

The chlorination of La_2O_3 begins at temperatures above 260 °C and leads to the formation of solid LaOCl. At temperatures above 850 °C, the lanthanum oxychloride is chlorinated to lanthanum trichloride, but the rate for the $LaCl_3(l)$ production is lower than its evaporation rate and thermo-gravimetric experiments show a loss of mass. Kinetic analysis showed that the reaction is under chemical control for temperatures below 325 °C. The formation of LaOCl proceeds through a nucleation and growth mechanism, and the conversion curves were analyzed with the Johnson−Mehl−Avrami description. The JMA parameters obtained were $n = 1.46$ and $E_a = 113$ kJ/mol. According to the JMA description and SEM images, the value of n is consistent with a three-dimensional growth and site saturation nucleation of the LaOCl phase. An overall rate equation was obtained, which includes the effects of the parameters analyzed (a pre-exponential factor was obtained for each temperature by combining eqs IV, XI, and XII and calculating the average):

$$\frac{d\alpha}{dt} = 1.2 \times 10^6 (\text{seg}\cdot\text{kPa}^{0.23})^{-1} \exp\left(-\frac{112\ \text{kJ/mol}}{R_g T}\right) \times p\text{Cl}_2{}^{0.23}\{1.46(1-\alpha)[-\ln(1-\alpha)]\}^{0.3}$$

AUTHOR INFORMATION

Corresponding Author

*E-mail: gaviriaj@cab.cnea.gov.ar. Phone: +54 02 94 444 5100. Fax: +54 02 94 444 5293.

Notes

The authors declare no competing financial interest.

ACKNOWLEDGMENTS

The authors thank the Agencia Nacional de Promoción Científica y Tecnológica (ANPCyT), Consejo Nacional de Investigaciones Científicas y Técnicas (CONICET), and Universidad Nacional del Comahue for the financial support.

REFERENCES

(1) Gimenes, M.; Oliveira, H. *Metall. Trans. B* **2001**, *32*, 1007−1013.
(2) Sun, Y-H; Wang, Z-C; Guo, L. *J. Alloys Compd.* **1999**, *285*, 73−76.
(3) Murase, K.; Machida, K-I; Adachi, G.-Y. *J. Alloys Compd.* **1995**, *217*, 218−225.
(4) Zhu, G-C; Li, F-P; Xiao, M.-G. *Trans. Nonferrous Met. Soc. China* **2003**, *13*, 1454−1458.
(5) Shi, W-Z; Zhang, X.; Zhao, Y-H; Wang, J-Y; Zhu, G.-C. *Chin. J. Process Eng.* **2005**, *5*, 23−28.
(6) Weckhuysen, B. M.; Rosynek, M. P.; Lunsford, J. H. *Phys. Chem. Chem. Phys.* **1999**, *1*, 3157−3162.
(7) Weckhuysen, B. M. *Phys. Chem. Chem. Phys.* **2003**, *5*, 4351−4360.

(8) van der Avert, P.; Podkolzin, S. G.; Manoilova, O.; de Winne, H.; Weckhuysen, B. M. *Chem.—Eur. J.* **2004**, *10*, 1637−1646.
(9) Van der Avert, P.; Weckhuysen, B. M. *Phys. Chem. Chem. Phys.* **2004**, *6*, 5256−5262.
(10) Podkolzin, S. G.; Manoilova, O. V.; Weckhuysen, B. M. *J. Phys. Chem. B* **2005**, *109*, 11634−11642.
(11) Esquivel, M. R.; Bohé, A. E.; Pasquevich, D. M. *Thermochim. Acta* **2003**, *398*, 81−91.
(12) Esquivel, M. R.; Bohé, A. E.; Pasquevich, D. M. *J. Mater. Process. Technol.* **2005**, *170*, 304−309.
(13) Esquivel, M. R.; Bohé, A. E.; Pasquevich, D. M. *Mater. Sci. Eng., A* **2005**, *397*, 310−313.
(14) Gaviría, J. P.; Bohé, A. E. *Metall. Trans. B* **2009**, *40*, 45−53.
(15) Julbe, A.; Chanaud, P.; Larbot, A.; Guizard, C.; Cot, L.; Mirodatos, C.; Borges, H. *Key Eng. Mater.* **1991**, *61/62*, 65−70.
(16) van der Heijden, A. W. A. M.; Bellière, V.; Espinosa Alonso, L.; Daturi, M.; Manoilova, O. V.; Weckhuysen, B. M. *J. Phys. Chem. B* **2005**, *109*, 23993−24001.
(17) van der Heijden, A. W. A. M.; Mens, Ad J. M.; Bogerd, R.; Weckhuysen, B. M. *Catal. Lett.* **2008**, *122*, 238−246.
(18) Podkolzin, S. G.; Stangland, E. E.; Jones, M. E.; Peringer, E.; Lercher, J. A. *J. Am. Chem. Soc.* **2007**, *129* (9), 2569−2576.
(19) Afanasiev, P.; Aouine, M.; Deranlot, C.; Epicier, T. *Chem. Mater.* **2010**, *22*, 5411−5419.
(20) Chen, Y.; Qian, Q.; Liu, X.; Xiao, L.; Chen, Q. *Mater. Lett.* **2010**, *64*, 6−8.
(21) Marsal, A.; Dezanneau, G.; Cornet, A.; Morante, J. R. *Sens. Actuators, B* **2003**, *95*, 266−270.
(22) Marsal, A.; Rossinyol, E.; Bimbela, F.; Tellez, C.; Coronas, J.; Vornet, A.; Morante, J. R. *Sens. Actuators, B* **2005**, *109*, 38−43.
(23) Pasquevich, D. M.; Caneiro, A. M. *Thermochim. Acta* **1989**, *156*, 275−283.
(24) Joint Committee for Powder Diffraction Standards, Powder Diffraction File, International Center for Diffraction Data, Swarthmore, PA.
(25) Neumann, A.; Walter, D. *Thermochim. Acta* **2006**, *445*, 200−204.
(26) Barin, I. *Thermochemical Data of Pure Substances*; VCH Verlags Gesellschaft: Weinheim, Germany, 1993.
(27) Baev, A. K.; Novikov, G. I. *Russ. J. Inorg. Chem.* **1965**, *10* (11), 1337−1341.
(28) HSC 6.12, Chemistry for Windows, Outukumpu Research Oy, Pori, Finland, 2006.
(29) Peringer, E.; Tejuja, C.; Salzinger, M.; Lemonidou, A. A.; Lercher, J. A. *Appl. Catal., A* **2008**, *350*, 178−185.
(30) Gaviría, J. P.; Bohé, A. E. *Thermochim. Acta* **2010**, *509*, 100−110.
(31) Gaviría, J. P.; Fouga, G. G.; Bohé, A. E. *Thermochim. Acta* **2011**, *517*, 24−33.
(32) Hills, A. W. D. *Metall. Trans. B* **1978**, *9*, 121−128.
(33) Ranz, W. E.; Marshall, W. R. Jr. *Chem. Eng. Prog.* **1952**, *48* (3), 141−146.
(34) Ranz, W. E.; Marshall, W. R. Jr. *Chem. Eng. Prog.* **1952**, *48* (4), 173−180.
(35) Geiger, G. H.; Poirier, D. R. *Transport Phenomena in Metallurgy*; Addison-Wesley: Reading, MA, 1973.
(36) Szekely, J.; Evans, J. W.; Sohn, H. Y. *Gas-Solid Reactions*; Academic Press: New York, 1976.
(37) Hakvoort, G. *Thermochim. Acta* **1994**, *233*, 63−73.
(38) Pasquevich, D. M. Ph.D. Thesis, Facultad de Ciencias Exactas de la Universidad Nacional de La Plata, La Plata, Argentina, 1990.
(39) Pasquevich, D. M.; Amorebieta, V. *Ber. Bunsen-Ges. Phys. Chem.* **1992**, *96* (4), 534−541.
(40) Avrami, M. J. *Chem. Phys.* **1939**, *7* (12), 1103−1113.
(41) Avrami, M. J. *Chem. Phys.* **1940**, *8* (2), 212−224.
(42) Avrami, M. J. *Chem. Phys.* **1941**, *9* (2), 177−184.
(43) Johnson, W. A.; Mehl, R. F. *Trans. Am. Inst. Min. Metall. Eng.* **1939**, *135*, 416−427.
(44) Kempen, A. T. W.; Sommer, F.; Mittemeijer, E. J. *J. Mater. Sci.* **2002**, *37* (2), 1321−1332.